

DIVISÃO DE PROGRAMAS DE PÓS-GRADUAÇÃO

DISSERTAÇÃO DE MESTRADO

**ROBUST 3D GRAVITY GRADIENT INVERSION BY
PLANTING ANOMALOUS DENSITIES**

Leonardo Uieda

Orientadora
Valéria Cristina Ferreira Barbosa

Rio de Janeiro
2011

ROBUST 3D GRAVITY GRADIENT INVERSION BY PLANTING ANOMALOUS
DENSITIES

Leonardo Uieda

TESE SUBMETIDA AO CORPO DOCENTE DO PROGRAMA DE PÓS-GRADUAÇÃO
EM GEOFÍSICA DO OBSERVATÓRIO NACIONAL COMO PARTE DOS REQUISITOS
NECESSÁRIOS PARA A OBTENÇÃO DO GRAU DE MESTRE EM GEOFÍSICA.

Aprovada por:

Dra. Valéria Cristina Ferreira Barbosa (Orientadora)

Dr. João Batista Corrêa da Silva

Dr. Eder C. Molina

Dr. Irineu Figueiredo

Dr. Cosme Ferreira da Ponte Neto (Suplente)

Dr. Julíio César S. O. Lyrio (Suplente)

RIO DE JANEIRO - BRASIL

2011

Ficha catalográfica – Biblioteca do ON

U33 Uieda, Leonardo.
Robust 3D gravity gradient inversion by planting
anomalous densities ./Leonardo Uieda.-Rio de Janeiro:Observatório Nacional, 2011.
45p.

Dissertação (Mestrado em Geofísica)- Observatório
Nacional, Rio de Janeiro, 2011.

1.Inversão.2. Gradiometria gravimétrica.I.Título.

CDU 550.3

SUMÁRIO

Resumo	3
Abstract	5
Introduction	7
Methodology	14
Planting algorithm	19
Lazy evaluation of the Jacobian matrix	22
Presence of non-targeted sources	23
Applications to synthetic data	27
Multiple targeted sources	27
Multiple targeted and non-targeted sources	28
Application to real data	34
Conclusions	39
Acknowledgments	41
References	42

**ROBUST 3D GRAVITY GRADIENT INVERSION BY
PLANTING ANOMALOUS DENSITIES**

Leonardo Uieda¹ and Valéria C. F. Barbosa¹

¹ Observatório Nacional, Geophysics Department, Rio de Janeiro, Brazil., E-mail:

leouieda@gmail.com; valcris@on.br

RESUMO

Desenvolvemos um novo método de inversão de dados de gradiometria gravimétrica para estimar uma distribuição de contrastes de densidade 3D definida em uma malha de prismas retangulares. O método proposto consiste em um algoritmo iterativo que não requer a solução de um sistema de equações. Ao contrário, a solução cresce sistematicamente em torno de prismas pre-especificados pelo usuário, chamados “sementes”, cujos contrastes de densidade são especificados a priori pelo intérprete. Podemos especificar um contraste de densidade diferente para cada semente, permitindo assim a interpretação de múltiplas fontes com contrastes de densidade variados e que produzem efeitos gravitacionais interferentes. Em situações reais, algumas das fontes podem não ser alvos geológicos de interesse à interpretação. Para lidar com essa restrição, desenvolvemos um procedimento robusto que não requer que o efeito gravitacional produzido pelas fontes geológicas que são alvos de interesse na interpretação seja separado em um pré-processamento antes da inversão. Este procedimento também não exige que haja informação a priori disponível sobre as fontes geológicas que não são alvos da interpretação. Em nosso algoritmo, as fontes estimadas crescem iterativamente através da acreção de prismas na periferia da estimativa em curso. Logo, somente as colunas da matriz Jacobiana que correspondem aos prismas na periferia da solução atual são necessárias para efetuar o cálculo do vetor de resíduos. Desta forma, as colunas individuais da Jacobiana devem ser calculadas somente quando

necessárias e descartadas após a acreção do respectivo prisma. Este procedimento, denominado “avaliação preguiçosa” na ciência da computação, reduz significantemente a demanda de memória do computador e tempo de processamento. Testes com dados sintéticos mostram a habilidade de nosso método em recuperar corretamente a geometria das fontes alvo, mesmo havendo efeitos gravitacionais interferentes produzidos por fontes geológicas que não são alvos de interesse. A inversão de dados de aerogradiometria gravimétrica coletados sobre o Quadrilátero Ferrífero, sudeste do Brasil, estimou corpos alongados compactos de minério de ferro que estão de acordo com informações sobre a geologia local e interpretações anteriores.

ABSTRACT

We have developed a new gravity gradient inversion method for estimating a 3D density-contrast distribution defined on a grid of rectangular prisms. Our method consists in an iterative algorithm that does not require the solution of a system of equations. Instead, the solution grows systematically around user-specified prismatic elements, called “seeds”, with given density contrasts. Each seed can be assigned a different density-contrast value, allowing the interpretation of multiple sources with different density contrasts and that produce interfering gravitational effects. In real world scenarios, some sources might not be targeted for the interpretation. Thus, we developed a robust procedure that requires neither the isolation of the gravitational effect of the targeted sources prior to the inversion, nor prior information about the non-targeted sources. In our iterative algorithm, the estimated sources grow by the accretion of prisms in the periphery of the current estimate. As a result, only the columns of the Jacobian matrix corresponding to the prisms in the periphery of the current estimate are needed for the computations. Therefore, the individual columns of the Jacobian can be calculated on demand and deleted after an accretion takes place, greatly reducing the demand for computer memory and processing time. Tests on synthetic data show the ability of our method to correctly recover the geometry of the targeted sources, even when interfering gravitational effects produced by non-targeted sources are present. By inverting the data from an airborne gravity gradiometry survey flown over the iron ore

province of Quadrilátero Ferrífero, southeastern Brazil, we estimate a compact iron ore body that agrees with the available geologic information and previous interpretations.

INTRODUCTION

Historically, the vertical component of the gravity anomaly has been widely used in exploration geophysics due to technological restrictions and to the simplicity of its measurement and interpretation. This fact propelled the development of a large variety of gravity inversion methods. Conversely, the technological difficulties in the acquisition of accurate airborne gravity gradiometry data resulted in a delay in the development of methods for the inversion of this kind of data. Consequently, before the early 1990s, few papers published in the literature were devoted to the interpretation (or analysis) of gravity gradiometer data. In this respect, two papers deserve the general readers' attention. The first is Vasco (1989) which presents a comparative study of the vertical component of gravity and the gravity gradient tensor by analyzing the resolution and covariance matrices of the interpretation model parameters resulting from the use of each type of data. The second paper is Pedersen and Rasmussen (1990) which studied data of gravity and magnetic gradient tensors and introduced scalar invariants that indicate the dimensionality of the sources.

Recent technological developments in designing and assembling moving-platform gravity gradiometers made it feasible to accurately measure the independent components of the gravity gradient tensor. These technological advances, paired with the advent of global positioning systems (GPS), have opened a new era in the acquisition of accurate airborne gravity gradiometry data. Thus, airborne gravity gradiometry became a useful tool for interpreting

geologic bodies present in both mining and hydrocarbon exploration areas. Gravity gradiometry has the advantage, compared with other gravity methods, of being extremely sensitive to localize density contrasts within regional geological settings (Zhdanov et al., 2010b).

Recently, some gravity gradient inversion algorithms have been adapted to predominantly interpret both: orebodies that are important mineral exploration targets (e.g., Li 2001; Zhdanov et al., 2004; Martinez et al., 2010; Wilson et al., 2011), and salt bodies in a sedimentary setting (e.g., Jorgensen and Kisabeth, 2000; Routh et al, 2001). All these methods discretize the Earth's subsurface into prismatic cells with homogeneous density contrasts and estimate a 3D density-contrast distribution, thus retrieving an image of geologic bodies. Usually, a gravity gradient data set contains a huge volume of observations of the five linearly independent tensor components. These observations are collected every few meters in surveys that may contain hundreds to thousands of line kilometers. This massive data set combined with the discretization of the Earth's subsurface into a fine grid of prisms results in a large-scale 3D inversion with hundreds of thousands of parameters and tens of thousands of data.

The solution of a large-scale 3D inversion requires overcoming two main obstacles. The first one is the large amount of computer memory required to store the matrices used in the computations, particularly the sensitivity matrix. The second obstacle is the CPU time required for matrix-vector multiplications and to solve the resulting linear system. One approach to overcome these problems is to use the fast Fourier transform for matrix-vector multiplications by exploiting the translational invariance of the kernels to reduce the linear

operators to Toeplitz block structure (Pilkington, 1997; Zhdanov et al., 2004; Wilson et al., 2011). However, these approaches are unable to deal with data on an irregular grid or on an uneven surface. Furthermore, the observations must lie above the surface topography, so these approaches cannot be applied to borehole data. Another strategy for the solution of large-scale 3D inversions uses a variety of data compression techniques. Portniaguine and Zhdanov (2002) use a compression technique based on cubic interpolation. Li and Oldenburg (2003) use a 3D wavelet compression on each row of the sensitivity matrix. Most recently, an alternative strategy for the solution of large-scale 3D inversion has been used under the name of “moving footprint” (Cox et al., 2010; Zhdanov et al., 2010a; Wilson et al., 2011). In this approach the full sensitivity matrix is not computed; rather, for each row, only the few elements that lie within the radius of the footprint size are calculated. In other words, the j th element of the i th row of sensitivity matrix only needs to be computed if its distance from the i th observation is smaller than a pre-specified footprint size (expressed in kilometers). The footprint size is a threshold value defined by the user and will depend on the natural decay of the Green's function for the gravity field. The smaller the footprint size, the larger the number of null elements in the rows of the sensitivity matrix; hence the faster the inversion and the greater the loss of accuracy. The user can then either accept the result or increase the footprint size and restart the inversion. This procedure leads to a sparse representation of the sensitivity matrix allowing the solution of otherwise intractable large-scale 3D inversions via the conjugate gradient technique.

Inversion methods for estimating a 3D density-contrast distribution that

discretize the Earth's subsurface into prismatic cells can produce either blurred images (e.g., Li and Oldenburg, 1998) or sharp images of the anomalous sources (Portniaguine and Zhdanov, 1999; Zhdanov et al., 2004; Silva Dias et al., 2009 and 2011). Nevertheless, all of the above-mentioned methods require the solution of a large linear system, which is, as pointed out before, one of the biggest computational hurdles for large-scale 3D inversions. Alternatively, there is a class of gravity inversion methods that do not solve linear systems but instead search the space of possible solutions for an optimum one. This class can be further divided into methods that use random search and those that use systematic search algorithms. Among the methods that use random search, we draw attention to the two following methods. Nagihara and Hall (2001) estimate a 3D density-contrast distribution using the simulated annealing algorithm (SA). Krahenbuhl and Li (2009) retrieve a salt body subject to density contrast constraints by developing a hybrid algorithm that combines the genetic algorithm (GA) with a modified form of SA as well as a local search technique that is not activated at every generation of the GA. On the other hand, an example of method that uses a systematic search is the method of Camacho et al. (2000). This method estimates a 3D density-contrast distribution using a systematic search to iteratively "grow" the solution, one prismatic element at a time, from a starting distribution with zero density contrast. At each iteration a new prismatic element is added to the estimate with a pre-specified positive or negative density contrast. This new prismatic element is chosen by systematically searching the set of all prisms that still have zero density contrast for the one whose incorporation into the estimate minimizes a goal function composed of the data-

misfit function plus the ℓ_2 -norm of the weighted 3D density-contrast distribution. Also belonging to the class of systematic search methods is René (1986), which is able to recover 2D compact bodies (i.e., with no holes inside) with sharp contacts by successively incorporating new prisms around user-specified prisms called “seeds” with the same given density contrast. At the first iteration, the new prism that will be incorporated is chosen by systematically searching the set of neighboring prisms of the seeds for the one that minimizes the data-misfit function. From the second iteration on, the search is performed over the set of available neighboring prisms of the current estimate. Thus, the solution grows through the addition of prisms to its periphery, in a manner mimicking the growth of crystals. In René's (1986) method, the estimated solution can be allowed to grow along any combinations of user-specified directions.

These inversion methods that do not solve linear systems have been applied to the vertical component of the gravity field yielding good results. To our knowledge, such class of methods has not been previously applied to interpret gravity gradiometry data. Besides, these methods are unable to deal with the presence of interfering gravitational effects produced by non-targeted sources, henceforth referred to as geological noise. This is a common scenario encountered in complex geological settings where the gravitational effect of non-targeted sources cannot be completely removed from the data. In the literature, few inversion methods have addressed this issue of interpreting only targeted sources when in the presence of non-targeted sources in a geologic setting (e.g., Silva and Holmann, 1983; Silva and Cutrim, 1989; Silva Dias et al., 2007). The

typical approach is to require the interpreter to perform some sort of data preprocessing in order to remove the gravitational effect produced by the non-targeted geologic sources. This preprocessing generally involves filtering the observed data based on the assumed spectral content of the targeted sources. However, separating the gravitational effect of multiple sources is often impractical, if not impossible without further information about the sources. An effective way to overcome this problem is to devise an inversion method that simultaneously estimates targeted geologic sources and eliminates the undesired effects produced by the non-targeted sources by means of a robust data-fitting procedure. Silva and Holmann (1983) and Silva and Cutrim (1989), for example, minimized, respectively, the ℓ_1 -norm and the Cauchy-norm of the residuals (the difference between the observed and predicted data) to take into account the presence of non-targeted sources. Both data-fitting procedures are more robust than the typical least-squares approach of minimizing the ℓ_2 -norm of the residuals, because they allow the presence of large residual values.

We present a new gravity gradient inversion for estimating a 3D density-contrast distribution belonging to the class of methods that do not solve linear systems, but instead implement a systematic search algorithm. Like René (1986), we incorporate prior information into the solution using seeds (i.e., user-specified prismatic elements) around which the solution grows. In contrast with René's (1986) method, our approach can be used to interpret multiple geologic sources because it allows assigning a different density contrast to each seed. We impose compactness on the solution using a modified version of the regularizing

function proposed by Silva Dias et al. (2009). We use as a data-misfit function either the ℓ_2 -norm or the ℓ_1 -norm of the residuals. Because the ℓ_1 -norm tolerates large data residuals, it can be used to eliminate the influence of the non-targeted sources in the data predicted by the estimate. Therefore, our approach requires neither prior information about the non-targeted sources nor a preprocessing of the data to isolate the effect of the targeted sources. Finally, we exploit the fact that our systematic search is limited to the neighboring prisms of the current estimate to implement a lazy evaluation of the sensitivity matrix, thus achieving a fast and memory efficient inversion. Tests on synthetic data and on airborne gravity gradiometry data collected over the Quadrilátero Ferrífero, southeastern Brazil, confirmed the potential of our method in producing sharp images of the targeted anomalous density distribution (iron orebody) in the presence of non-targeted sources.

METHODOLOGY

Let $\mathbf{g}^{\alpha\beta}$ be an $L \times 1$ vector that contains observed values of the $g_{\alpha\beta}$ component of the gravity gradient tensor (Figure 1a and b), where α and β belong to the set of x -, y -, and z - directions of a right-handed Cartesian coordinate system (Figure 1c). We assume that $\mathbf{g}^{\alpha\beta}$ is caused by an anomalous density contrast distribution contained within a three-dimensional region of the subsurface. This region can be discretized into M juxtaposed 3D right rectangular prisms composing the assumed interpretation model. Each prism of this model has a homogeneous density contrast and the resulting piecewise-constant anomalous density contrast distribution is assumed to be sufficient to approximate the true one. It follows that the $g_{\alpha\beta}$ produced by the anomalous density contrast distribution can be approximated by the sum of the contributions of each prism of the interpretation model, i.e.,

$$\mathbf{d}^{\alpha\beta} = \sum_{j=1}^M p_j \mathbf{a}_j^{\alpha\beta} . \quad (1)$$

This linear relationship can be written in matrix notation as

$$\mathbf{d}^{\alpha\beta} = \mathbf{A}^{\alpha\beta} \mathbf{p} , \quad (2)$$

where \mathbf{p} is an M -dimensional vector whose j th element, p_j , is the density contrast of the j th prism of the interpretation model, $\mathbf{d}^{\alpha\beta}$ is an L -dimensional vector of data predicted by \mathbf{p} , which presumably approximates $\mathbf{g}^{\alpha\beta}$, and $\mathbf{A}^{\alpha\beta}$ is the $L \times M$ Jacobian (or sensitivity) matrix, whose j th column is the L -

dimensional vector $\mathbf{a}_j^{\alpha\beta}$. The i th element of $\mathbf{a}_j^{\alpha\beta}$ is numerically equal to the $g_{\alpha\beta}$ component of the gravity gradient tensor caused by the j th prism of the interpretation model, with unit density contrast, calculated at the place where the i th observation was made. It is then evident that the j th column of the Jacobian matrix represents the influence that p_j has on the predicted data. The elements of matrix $A^{\alpha\beta}$ can be calculated using the formulas of Nagy et al. (2000).

In cases where more components of the gravity gradient tensor are available, we can concatenate the observed data vectors $\mathbf{g}^{\alpha\beta}$ into a single $N \times 1$ vector \mathbf{g} of all observed data,

$$\mathbf{g} = [\mathbf{g}^{xx \ T} \ \mathbf{g}^{xy \ T} \ \mathbf{g}^{xz \ T} \ \mathbf{g}^{yy \ T} \ \mathbf{g}^{yz \ T} \ \mathbf{g}^{zz \ T}]^T, \quad (3)$$

where the superscript T denotes transposition. Likewise, we can define an $N \times M$ Jacobian matrix,

$$\mathbf{A} = \begin{bmatrix} \mathbf{A}^{xx} \\ \mathbf{A}^{xy} \\ \mathbf{A}^{xz} \\ \mathbf{A}^{yy} \\ \mathbf{A}^{yz} \\ \mathbf{A}^{zz} \end{bmatrix}, \quad (4)$$

and an N -dimensional vector of predicted data,

$$\mathbf{d} = [\mathbf{d}^{xx \ T} \ \mathbf{d}^{xy \ T} \ \mathbf{d}^{xz \ T} \ \mathbf{d}^{yy \ T} \ \mathbf{d}^{yz \ T} \ \mathbf{d}^{zz \ T}]^T. \quad (5)$$

The predicted data vector \mathbf{d} is related to the Jacobian matrix \mathbf{A} and the density-contrast distribution \mathbf{p} through the linear system,

$$\mathbf{d} = \mathbf{A} \mathbf{p} = \sum_{j=1}^M p_j \mathbf{a}_j, \quad (6)$$

where \mathbf{a}_j is the $N \times 1$ vector corresponding to the j th column of matrix \mathbf{A} .

Note that if not all components of the gravity gradient tensor are available, the missing components must be left out of matrix \mathbf{A} and of vectors \mathbf{g} and \mathbf{d} .

We formulate the inverse problem as the estimation of the parameter vector \mathbf{p} that minimizes the data-misfit function $\phi(\mathbf{p})$, defined as a norm of the N -dimensional residual vector \mathbf{r} . The residual vector is the difference between the observed and predicted data vectors, \mathbf{g} and \mathbf{d} , i.e.,

$$\mathbf{r} = \mathbf{g} - \mathbf{d}. \quad (7)$$

For a least-squares fit, $\phi(\mathbf{p})$ is defined as the ℓ_2 -norm of the residual vector, i.e.,

$$\phi(\mathbf{p}) = \|\mathbf{r}\|_2 = \left(\sum_{i=1}^N (g_i - d_i)^2 \right)^{\frac{1}{2}}. \quad (8)$$

The least-squares fit distributes the residuals assuming that the errors in the data follow a short-tailed Gaussian distribution and thus large residual values are highly improbable (Claerbout and Muir, 1973; Silva and Holmann, 1983; Menke, 1989; Tarantola, 2005). Hence, the ℓ_2 -norm is sensitive to outliers in the data, which can result from either gross errors or geological noise (i.e., anomalous density contrasts which are not of interest to the interpretation). On the other hand, if occasional large residuals are desired in the inversion, one can use the ℓ_1 -norm of the residuals vector, i.e.,

$$\phi(\mathbf{p}) = \|\mathbf{r}\|_1 = \sum_{i=1}^N |g_i - d_i|. \quad (9)$$

In this case, the errors in the data are assumed to follow a long-tailed Laplace distribution and a more robust fit is obtained since the predicted data will be insensitive to outliers.

Regardless of the norm used in the data-misfit function $\phi(\mathbf{p})$, the inverse problem of minimizing $\phi(\mathbf{p})$ to estimate a three-dimensional density-contrast distribution is ill-posed and requires additional constraints to be transformed into a well-posed problem with a unique and stable solution. The constraints chosen for our method are:

1. the solution should be compact (i.e., without any holes inside it).
2. the excess (or deficiency) of mass in the solution should be concentrated around user-specified prisms of the interpretation model with known density contrasts (referred to as “seeds”).
3. the only density-contrast values allowed are zero or the values assigned to the seeds.
4. each element of the solution should have the density contrast of the seed closest to it.

We formulate the constrained inverse problem as the estimation of the parameter vector \mathbf{p} that minimizes the goal function

$$\Gamma(\mathbf{p}) = \phi(\mathbf{p}) + \mu \theta(\mathbf{p}), \quad (10)$$

where $\theta(\mathbf{p})$ is a regularizing function defined in the parameter (model) space that imposes physical and/or geological attributes on the solution. The scalar μ is a regularizing parameter that balances the trade-off between the data-misfit measure $\phi(\mathbf{p})$ and the regularizing function $\theta(\mathbf{p})$. The regularizing function

$\theta(\mathbf{p})$ is an adaptation of the one used in Silva Dias et al. (2009), which in turn is a modified version of the one used by Guillen and Menichetti (1984) and Silva and Barbosa (2006). It enforces the compactness of the solution and the concentration of mass around the seeds (i.e., constraints 1 and 2), being defined as

$$\theta(\mathbf{p}) = \sum_{j=1}^M \frac{p_j}{p_j + \epsilon} l_j^\beta , \quad (11)$$

where p_j is the j th element of \mathbf{p} , l_j is the distance between the center of the j th prism and the center of the closest seed (see subsection Planting algorithm), ϵ is a small positive scalar used to avoid a singularity when $p_j=0$, and β is a positive integer that influences how compact the solution will be. Typical values of β range from three to seven, depending on how much compactness one desires to impose. The larger the value of β , the closer to the seeds the estimated anomalous density contrasts will be. In practice, the scalar ϵ is not necessary because one can simply add either zero or l_j^β in the summation of equation 11 when evaluating the regularizing function.

The two remaining constraints (3 and 4) are imposed algorithmically. Our algorithm, named “planting algorithm”, requires that a set of N_s seeds and their associated density-contrast values be specified by the user. We emphasize that the density-contrast values of the seeds do not need to be the same. These seeds should be chosen according to prior information about the targeted anomalous density contrasts, such as those provided by the available geologic models, well logs and previous inversions. Our algorithm searches for the

minimum value of the data-misfit function (equations 8 and 9) and the lowest possible value of the goal function (equation 10) that still fits the data by iteratively performing the accretion of prisms with non-null density contrasts around the given set of seeds. These accreted prisms will have a density contrast equal to the one of the seed suffering the accretion, guaranteeing constraint 3. Furthermore, only the neighboring prisms of the current solution may be used in the accretion, guaranteeing constraint 4. This growth of the solution through successive accretions is controlled by the values of the data-misfit and goal functions. In addition, the planting algorithm does not require calculation of the derivative of the goal function, enabling the use of either the ℓ_2 - or ℓ_1 - norms of the residual vector (equations 8 and 9) without modification of the algorithm.

Planting algorithm

Given a set of N_s seeds (i.e., prisms of the interpretation model and their assigned density-contrast values), our algorithm starts with an initial parameter vector that includes the density-contrast values assigned to the seeds and has all other elements set to zero (Figure 2a). Hence, by combining equations 6 and 7, we define the initial residual vector as

$$\mathbf{r}^{(0)} = \mathbf{g} - \left(\sum_{s=1}^{N_s} \rho_s \mathbf{a}_{j_s} \right), \quad (12)$$

where ρ_s is the density contrast of the s th seed, j_s is the corresponding index of the s th seed in the parameter vector \mathbf{p} , and \mathbf{a}_{j_s} is the N -dimensional

column vector of the Jacobian matrix A corresponding to the s th seed.

The solution to the inverse problem is then built through an iterative growth process. An iteration of the growth process consists of attempting to grow, one at a time, each of the N_s seeds by performing the accretion of one of its neighboring prisms. We define the accretion of a prism as changing its density-contrast value from zero to the density contrast of the seed undergoing the accretion, guaranteeing constraint 3. Thus, a growth iteration is composed of at most N_s accretions, one for each seed. The choice of a neighboring prism for the accretion to the s th seed follows two criteria:

1. The addition of the neighboring prism to the current estimate should reduce the data-misfit function $\phi(\mathbf{p})$ (equations 8 or 9), as compared to the previous accretion. This ensures that the solution grows in a way that best fits the observed data. To avoid an exaggerated growth of the estimated anomalous density contrasts, the algorithm does not perform the accretion of neighboring prisms that produce very small changes in the data-misfit function. The criterion for how small a change is accepted is based on whether the following inequality holds:

$$\frac{|\phi^{(new)} - \phi^{(old)}|}{\phi^{(old)}} \geq \delta , \quad (13)$$

where $\phi^{(new)}$ is the data-misfit function evaluated with the chosen neighboring prism included in the estimate, $\phi^{(old)}$ is the data-fitting function evaluated during the previous accretion, and δ is a positive scalar typically ranging from 10^{-3} to 10^{-6} . Parameter δ controls how much the anomalous density contrasts are allowed to grow. The choice of

the value of δ depends on the size of the prisms of the interpretation model. The smaller the prisms are, the smaller their contribution to $\phi(\mathbf{p})$ will be and thus the smaller δ should be.

2. The addition of the neighboring prism with density contrast ρ_s to the current estimate should produce the smallest value of the goal function $\Gamma(\mathbf{p})$ (equation 10) out of all other neighboring prisms of the s th seed that obeyed the first criterion. Thus, the accretion of the neighboring prism to the current estimate will produce the highest decrease in the data-misfit function while increasing the regularizing function $\theta(\mathbf{p})$ as little as possible. This ensures that constraints 1, 2, and 4 are met. We recall here that the term l_j in equation 11 is the distance between the center of the j th prism and the center of the s th seed of which it is a neighboring prism.

Once an accretion of a neighboring prism is performed to the s th seed, its list of neighboring prisms is updated to include the neighboring prisms of the prism chosen for the accretion (Figure 2b). We also update the residual vector by

$$\mathbf{r}^{(new)} = \mathbf{r}^{(old)} - p_j \mathbf{a}_j , \quad (14)$$

where $\mathbf{r}^{(new)}$ is the updated residual vector, $\mathbf{r}^{(old)}$ is residual vector evaluated in the previous accretion, j is the index of the neighboring prism chosen for the accretion, $p_j = \rho_s$, and \mathbf{a}_j is the j th column vector of the Jacobian matrix \mathbf{A} . In the case that none of the neighboring prisms of the s th seed meet the first criterion, the s th seed does not grow during this growth iteration. This ensures

that different seeds can produce anomalous density contrasts that correspond to sources of different sizes. The growth process continues while at least one of the seeds is able to grow. At the end of the growth process, our planting algorithm should yield a solution composed of compact anomalous density contrasts with variable sizes (Figure 2c).

Lazy evaluation of the Jacobian matrix

In our planting algorithm all elements of the parameter vector not corresponding to the seeds start with zero density contrast. It is then noticeable from equations 6 and 12 that the columns of the Jacobian matrix that do not correspond to the seeds are not required for the initial computations. Moreover, the search for the next element of the parameter vector for the accretion is restricted to the neighboring prisms of the current solution. This means that the j th column vector \mathbf{a}_j of the Jacobian matrix only needs to be calculated once the j th prism of the interpretation model becomes eligible for accretion (i.e., becomes a neighboring prism of the current solution). In addition, our algorithm updates the residual vector after each successful accretion through equation 14 and consequently, once the j th prism is permanently incorporated into the current solution, column vector \mathbf{a}_j is no longer needed. Thus, the full Jacobian matrix \mathbf{A} is not needed at any single time during the growth process. Column vectors of \mathbf{A} can be calculated on demand and deleted once they are no longer required (i.e., after an accretion). This technique is known in computer science as a “lazy evaluation”. Since the computation of the full Jacobian matrix is a time-

and memory-consuming process, the implementation of a lazy evaluation of \mathbf{A} leads to small inversion times and low memory usage, making viable the inversion of large data sets using interpretation models composed of large numbers of prisms without needing supercomputers or data compression algorithms (e.g., Portniaguine and Zhdanov, 2002).

Presence of non-targeted sources

In real world scenarios there are interfering gravitational effects produced by multiple and horizontally separated sources (Figure 3a). Some of these sources may be of no interest to the interpretation (i.e., non-targeted sources) or there may be no available prior information on them, such as their approximate location or density contrasts. Furthermore, in most cases it is not possible to perform a previous separation of the gravitational effects of the targeted and the non-targeted sources. It would then be desirable to provide seeds only for the targeted sources and that the estimated density-contrast distribution could be obtained without being affected by the gravitational effects of the non-targeted sources. For this purpose, one can use the ℓ_1 -norm of the residual vector (equation 9) to allow large residual values in places where the gravitational effects of the non-targeted sources are dominant (Figure 3b). In this case, the inversion will be able to ignore effectively the gravitational effect yielded by the non-targeted sources by treating it as outliers in the data. This robust procedure allows one to choose the targets of the interpretation without having to isolate their gravitational effect before the performing the inversion. It also eliminates the need for prior information about the non-targeted sources. Note that this is only

possible because the constraints used in the inversion are imposed in a very strict way throughout the planting algorithm.

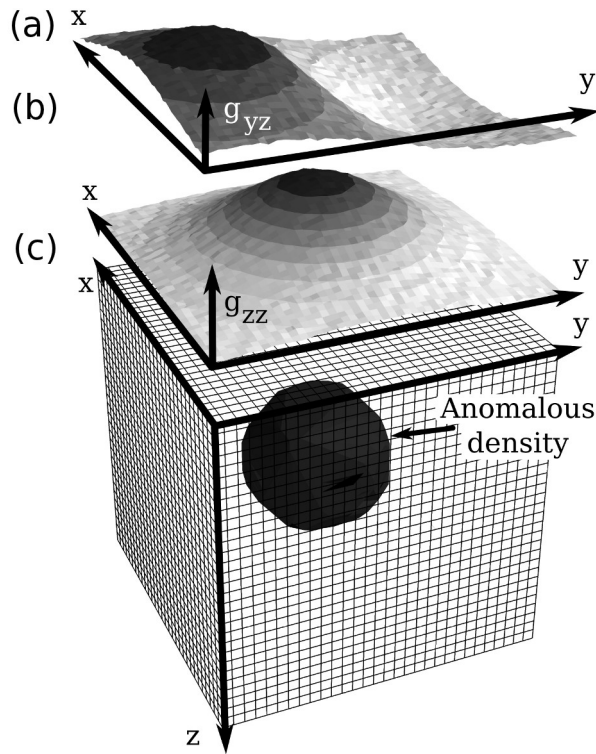


Figure 1. The observed (a) g_{yz} and (b) g_{zz} components of the gravity gradient tensor (shaded relief contour maps) produced by an anomalous density contrast distribution. (c) Schematic representation of the interpretation model consisting of a grid of M juxtaposed 3D right-rectangular prisms. The interpretation model is used to parameterize the anomalous density contrast distribution shown in gray.

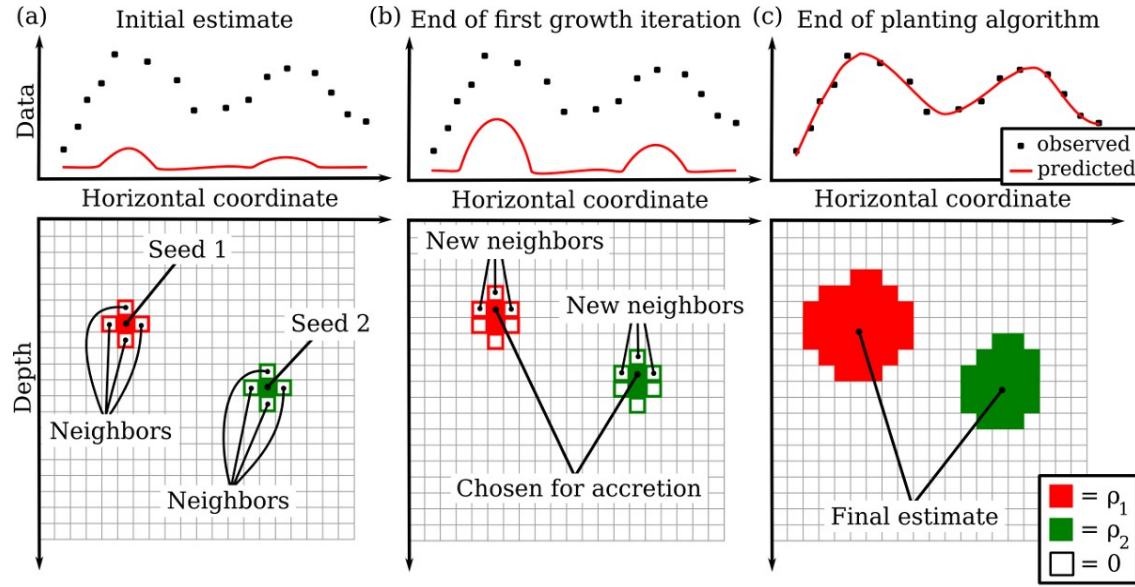


Figure 2. 2D sketch of three stages of the planting algorithm. Black dots represent the observed data and the red line represents the predicted data produced by the current estimate. The light gray grid of prisms represents the interpretation model. (a) Initial state with the user-specified seeds included in the estimate with their corresponding density contrasts and all other parameters set to zero. (b) End of the first growth iteration where two accretions took place, one for each seed. The list of neighboring prisms of each seed and the predicted data are updated. (c) Final estimate at the end of the algorithm. The growth process stops when the predicted data fits the observed data.

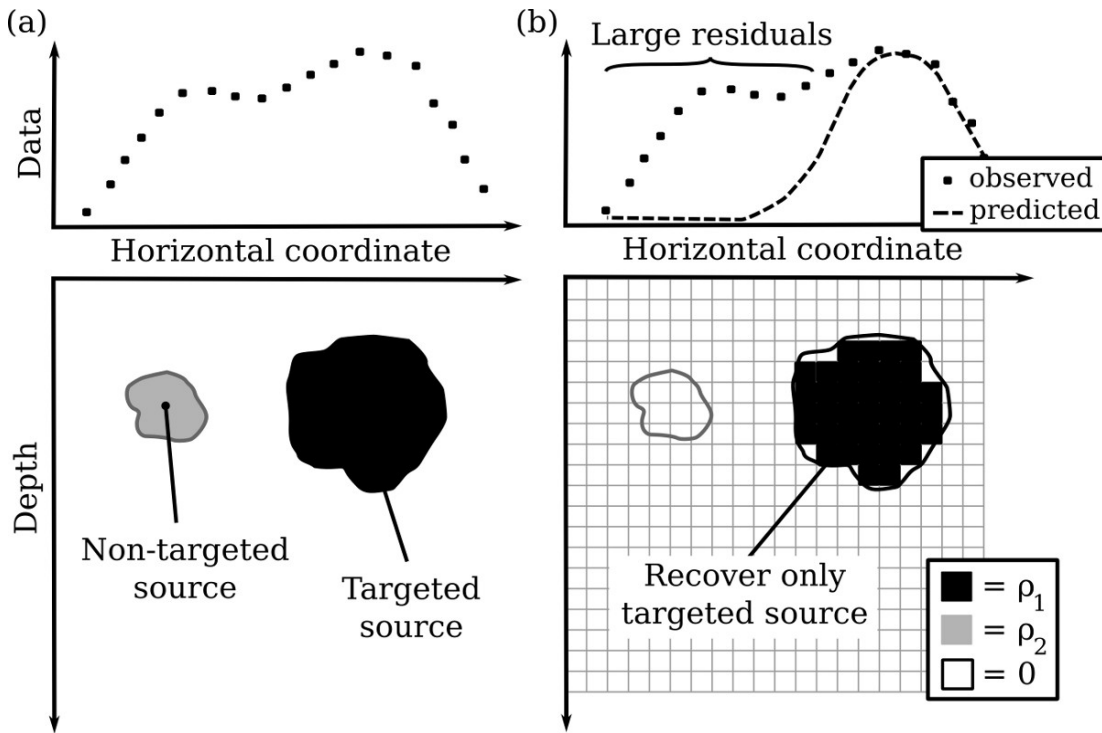


Figure 3. 2D sketch of the robust procedure. Black dots represent the observed data produced by (a) the true sources with different density contrasts (black and gray polygons). The source with density contrast ρ_2 (gray polygon) is considered as non-targeted. (b) Inversion result when a seed is given for the targeted source only (black polygon) and using the ℓ_1 -norm of the residual vector (equation 9). The dashed line in b represents the data predicted by the inversion result. Large residuals over the non-targeted source (gray outline) are automatically allowed by the inversion. The estimated density-contrast distribution (black prisms) recovers only the shape of the targeted source (black outline).

APPLICATIONS TO SYNTHETIC DATA

We present two applications to synthetic data that simulate airborne gravity gradiometry surveys over multiple homogeneous sources that are horizontally closely located and produce interfering gravitational effects. The sources are separated by abrupt contacts and have different density contrasts and geometries.

Multiple targeted sources

Figure 4 shows a set of color-scale maps of the synthetic noise-corrupted g_{xx} , g_{xy} , g_{xz} , g_{yy} , g_{yz} , and g_{zz} components of the gravity gradient tensor calculated at 150 meter height. The data were contaminated with pseudorandom Gaussian noise with zero mean and 5 Eötvös standard deviation. Each tensor component was calculated on a regular grid of 26×26 observation points in the x - and y -directions, totaling a data set of 4,056 observations, with a grid spacing of 0.2 km along both directions. The synthetic data simulate the noise-corrupted data from an airborne gravity gradiometry survey which were produced by four closely separated sources (Figure 5a). These sources are rectangular parallelepipeds with different sizes and depths and with density contrasts ranging from -1 g/cm^3 to 1 g/cm^3 .

In this test, all four sources are considered targets of the interpretation. Because we did not consider the presence of geologic noise (non-targeted sources), the inversion was performed using the ℓ_2 -norm of the residual vector

(equation 8) and specifying a total of 18 seeds (Figure 5b) distributed between the four sources as follows: seven for the source with density contrast of 1 g/cm^3 (in red); five for the source with density contrast of -1 g/cm^3 (in blue); four for the source with density contrast of 0.7 g/cm^3 (in yellow); two for the source with density contrast of 0.9 g/cm^3 (in orange). We adopted an interpretation model consisting of 25,000 juxtaposed right rectangular prisms and set $\beta=7$, $\mu=10^{15}$, and $\delta=5\times10^{-4}$. The inversion result in Figure 5c shows that our method estimates a density-contrast distribution composed of four compact sources (i.e., without holes in their interiors) whose shapes very closely resemble the shape of the four true sources shown in Figure 5a, regardless of their depth, size, or density contrast. This estimated density-contrast distribution fits the observed data as shown in Figure 4 in solid black lines.

Multiple targeted and non-targeted sources

Figure 6a-c shows the synthetic noise-corrupted g_{yy} , g_{yz} , and g_{zz} components of the gravity gradient tensor (color-scale maps) produced by 11 rectangular parallelepipeds (Figure 7a) with density contrasts ranging from -1 g/cm^3 to 1.2 g/cm^3 . Each component was calculated on a regular grid of 51×51 observation points in the x - and y -directions, totaling 7,803 observations, with a grid spacing of 0.1 km along both directions. We corrupted the synthetic data with pseudorandom Gaussian noise with zero mean and 5 Eötvös standard deviation.

To demonstrate the efficiency of our method in retrieving only the targeted

sources even in the presence of non-targeted ones, we chose only the sources with density contrast of 1.2 g/cm^3 (red blocks in Figure 7a) as targets of the interpretation. Thus, we specified the set of 13 seeds shown in Figure 7b (nine for the largest source and four for the smallest one) and used the ℓ_1 -norm of the residual vector (equation 9). In this interpretation, all sources with density contrast different from 1.2 g/cm^3 (displayed as blue and green blocks in Figure 7a) were considered as non-targeted sources. The inversion was performed using an interpretation model consisting of 37,500 juxtaposed rectangular prisms and $\beta=5$, $\mu=10^5$, and $\delta=10^{-4}$.

Figure 6a-c shows the predicted data (black contour lines) produced by the estimated density-contrast distribution shown in Figure 7c. By comparing the density contrast estimates (Figure 7c) with the true targeted sources (red blocks in Figure 7a), we verify the good performance of our method in recovering targeted sources in the presence of non-targeted sources (blue and green blocks in Figure 7a) yielding interfering gravitational effects. The most striking feature of this inversion result is that neither prior information about the non-targeted sources nor a gravitational effect separation to isolate the effect of the targeted sources were required. For comparison, Figure 6d-f shows, in colored-contour maps, the g_{yy} , g_{yz} , and g_{zz} components of the gravity gradient tensor produced by only the targeted sources (red blocks in Figure 7a) plotted against the predicted data (black contour lines in Figure 6a-f) produced by the estimated density-contrast distribution (Figure 7c). Notice that the inversion performed on the full synthetic data set (color-scale maps in Figure 6a-c) was able to fit the

isolated gravitational effects produced by the targeted sources as shown in Figure 6d-f. These results confirm the ability of our method to effectively ignore the interfering gravitational effect of non-targeted sources and successfully recover the targets of the interpretation.

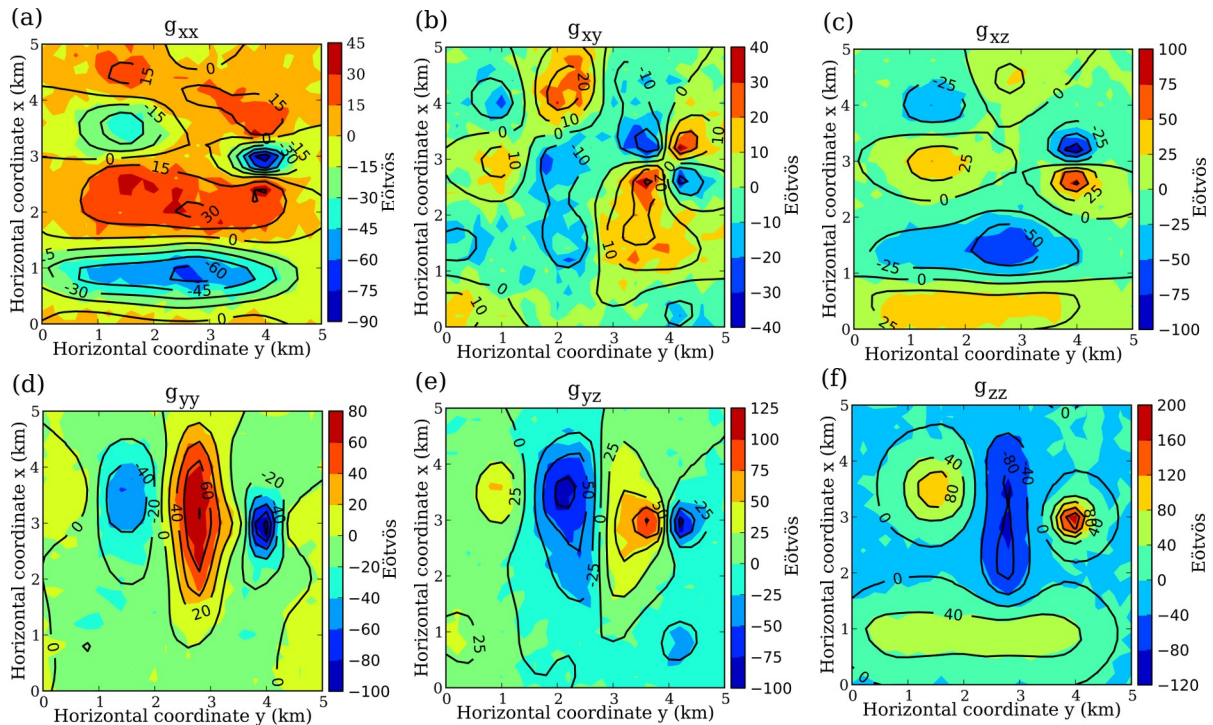


Figure 4. Test with synthetic data produced by multiple targeted sources.

Synthetic noise-corrupted data (color-scale maps) and data predicted by the inversion result (black contour lines) of the (a) g_{xx} , (b) g_{xy} , (c) g_{xz} , (d) g_{yy} , (e) g_{yz} , and (f) g_{zz} components of the gravity gradient tensor. The synthetic data are produced by the four prisms shown in Figure 5a. The predicted are produced by the estimated density-contrast distribution shown in Figure 5c.

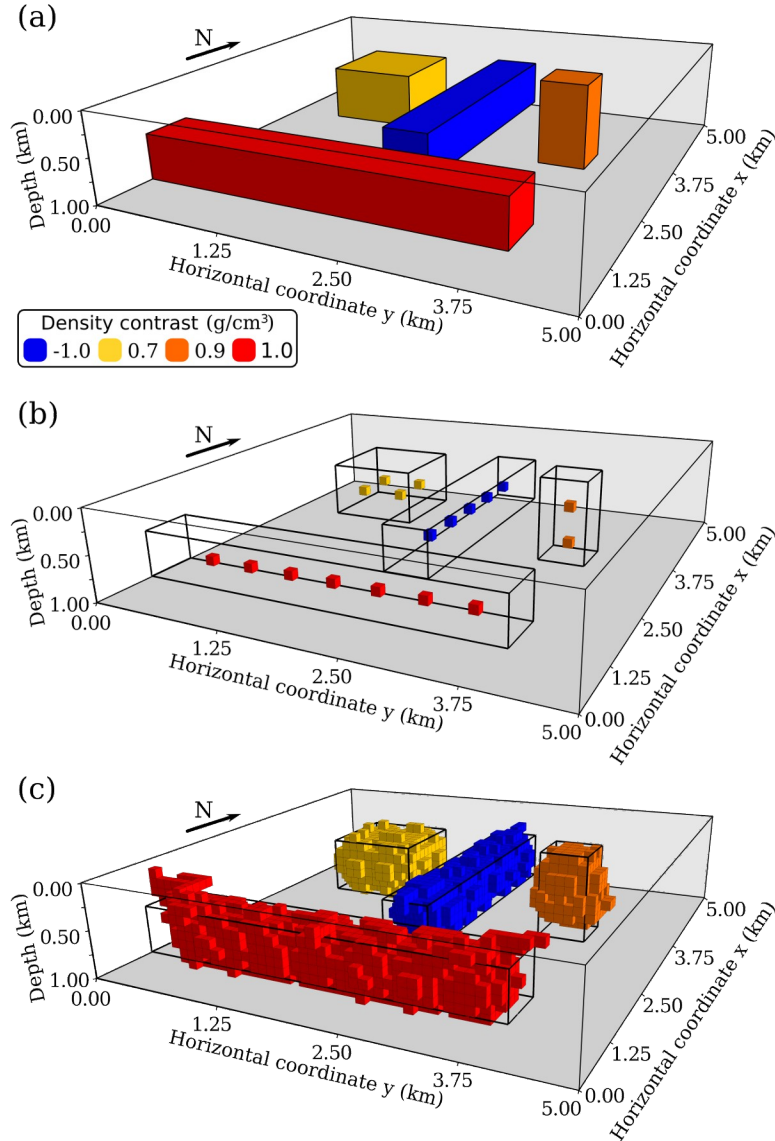


Figure 5. Test with synthetic data produced by multiple targeted sources. (a) Perspective view of the four targeted sources used to generate the synthetic data. (b) Seeds used in the inversion and outline of the true targeted sources. (c) Inversion result using the ℓ_2 -norm of the residual vector. Prisms of the interpretation model with zero density contrast are not shown. Black lines represent the outline of the true targeted sources.

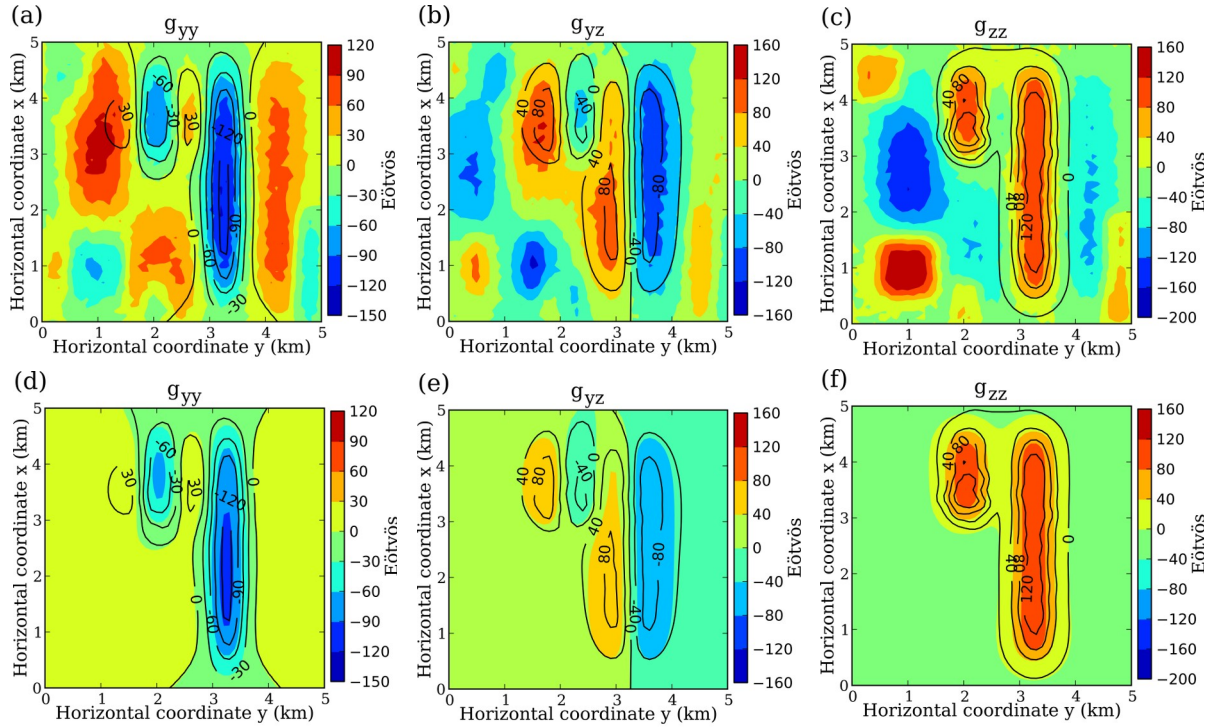


Figure 6. Test with synthetic data produced by multiple targeted and non-targeted sources. Synthetic noise-corrupted data (color-scale maps) and data predicted by the inversion result (black contour lines) of the (a) g_{yy} , (b) g_{yz} , and (c) g_{zz} components of the gravity gradient tensor. The synthetic data were produced by the 11 sources shown in Figure 7a. The predicted data is produced by the inversion result shown in Figure 7c. The (d) g_{yy} , (e) g_{yz} , and (f) g_{zz} components of the gravity gradient tensor produced only by the targeted sources are shown in color-scale maps and black contour lines show the same data predicted by the inversion result in Figure 7.

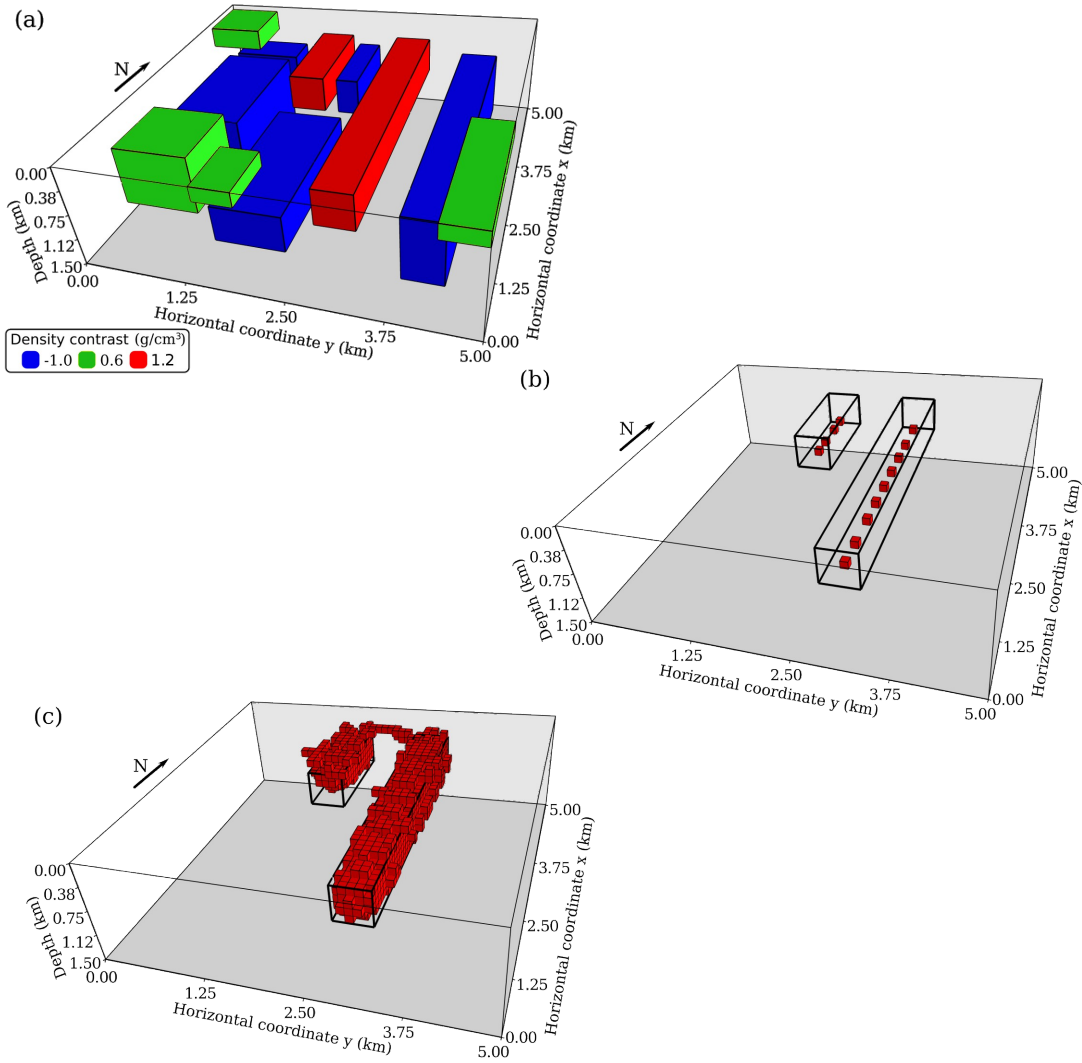


Figure 7. Test with synthetic data produced by multiple targeted and non-targeted sources. (a) Perspective view of the synthetic model used to generate the synthetic data. Only sources with density contrast 0.6 g/cm^3 (green) are outcropping. The sources with density contrast 1.2 g/cm^3 (red) were considered as the targets of the interpretation. (b) Seeds used in the inversion and outline of the true targeted sources. (c) Inversion result obtained by using the ℓ_1 -norm of the residual vector (equation 9). Prisms of the interpretation model with zero density contrast are not shown. Black lines represent the outline of the true targeted sources.

APPLICATION TO REAL DATA

One of the most important iron provinces in Brazil is the Quadrilátero Ferrífero (QF), located in the São Francisco Craton, southeastern Brazil. Most of the iron ore bodies in the QF are hosted in the oxidized, metamorphosed and heterogeneously deformed Banded Iron Formation (BIF) of the Cauê Formation, the so-called itabirites. The itabirites are associated with the Minas Supergroup and contain iron ore oxide facies, such as hematites, magnetites and martites. We applied our method to estimate the geometry and extent of the iron ore deposits of the Cauê Formation using the data from an airborne gravity gradiometry survey performed in this area (color-scale maps in Figure 8a-c). The gravitational effects associated with the iron ore bodies (targeted sources) are more prominent in the g_{yy} , g_{yz} , and g_{zz} components of the measured gravity gradient tensor (elongated SW-NE feature in Figure 8a-c). This data set also shows interfering gravitational effects caused by other sources, which will be considered non-targeted sources in our interpretation.

The inversion was performed on 4,582 measurements of each of the g_{yy} , g_{yz} , and g_{zz} components of the gravity gradient tensor resulting in a total of 13,746 measurements. We applied our robust procedure to recover only the targeted sources (iron ore bodies) in the presence of the non-targeted sources. Thus, we used the ℓ_1 -norm of the residual vector (equation 9) and provided a set of 46 seeds (black stars in Figure 8) for the targeted iron ore bodies of the Cauê Formation. The horizontal locations of the seeds were chosen based on the

peaks of the elongated SW-NE positive feature in the color-scale map of the g_{zz} component (Figure 8c). The depths of the seeds were chosen based on borehole information and previous geologic interpretations of the area (D. U. Carlos, personal communication, 2010). We assigned a density-contrast value of 1.0 g/cm³ for the seeds because the data were terrain corrected using a density of 2.67 g/cm³ and the assumed density of the iron ore deposits is 3.67 g/cm³. The interpretation model consists of a mesh composed of 164,892 prisms and follows the topography of the area (Figure 9a). The inversion was performed using parameters $\beta=7$, $\mu=10^{15}$, and $\delta=5\times10^{-5}$.

The estimated density-contrast distribution corresponding to the iron ore bodies is shown in red in Figure 9. Cross-sections of the estimated density contrast distribution (Figure 10) show that the estimated iron ore bodies are compact and have non-outcropping parts. Figure 8d-f shows the predicted data caused by the estimated density-contrast distribution shown in Figure 9. For all three components, the inversion is able to fit the elongated SW-NE feature associated with the iron ore deposits (targeted sources) and successfully ignore the other gravitational effects produced by the non-targeted sources (Figure 8). These results show the ability of our method to provide a compact estimate of the iron ore deposits. We emphasize that this was possible without any prior information about the non-targeted sources and without isolating the gravitational effects produced by the targeted sources. Meeting both of these requirements would have been impractical in this highly complex geological setting. Our results are in close agreement with previous interpretations by Martinez et al. (2010). Furthermore, when performed on a standard laptop computer with an Intel®

Core™ 2 Duo P7350 2.0 GHz processor, the total time for the inversion was approximately 14 minutes.

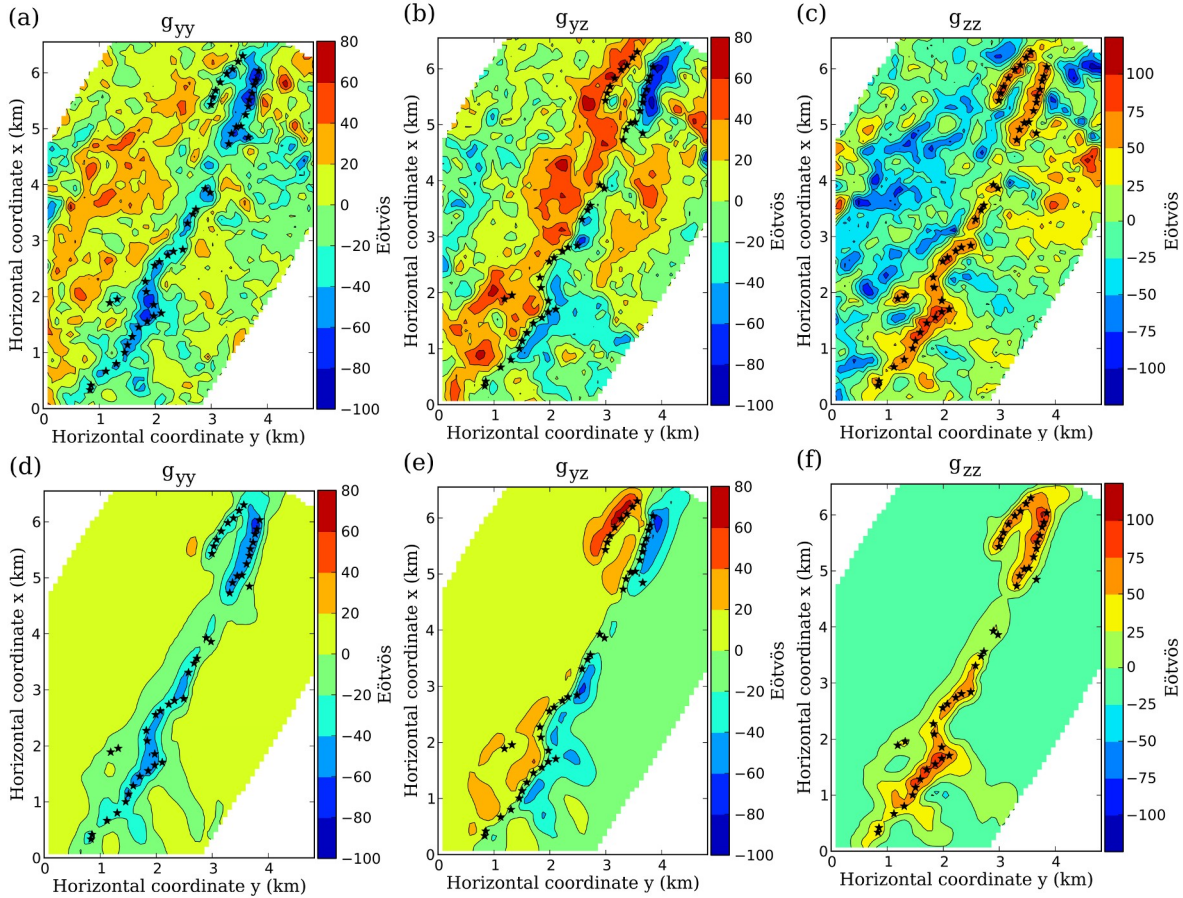


Figure 8. Application to real data from an airborne gravity gradiometry survey over a region of the Quadrilátero Ferrífero, southeastern Brazil. The observed (a-c) and predicted (d-f) g_{yy} , g_{yz} , and g_{zz} components of the gravity gradient tensor. The latter were produced by the estimated density-contrast distribution shown in Figure 9. Black stars represent the horizontal coordinates of the seeds used in the inversion.

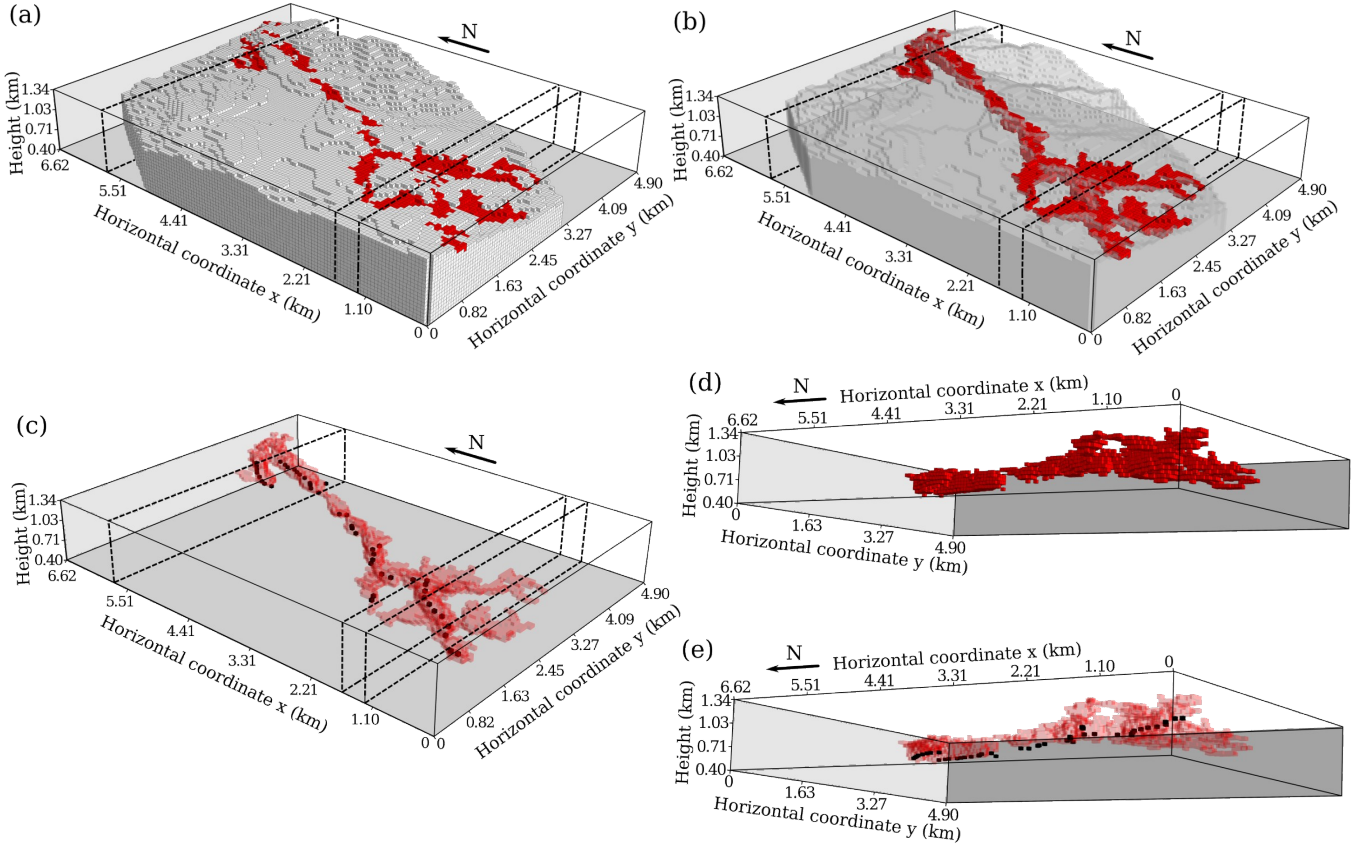


Figure 9. Results from the application to real data from the Quadrilátero Ferrífero, southeastern Brazil. The vertical axis refers to height above the ellipsoid. Dashed lines show the location of the cross-sections in Figure 10. (a-e) Perspective views of the estimated density-contrast distribution, where prisms with zero density contrast are shown in solid or transparent light gray and prisms with density contrast of 1.0 g/cm^3 are shown in solid or transparent red. The seeds used in the inversion are shown as black prisms. The estimated density-contrast distribution corresponding to the iron orebody of the Cauê itabirite are the red prisms with 1.0 g/cm^3 density contrast.

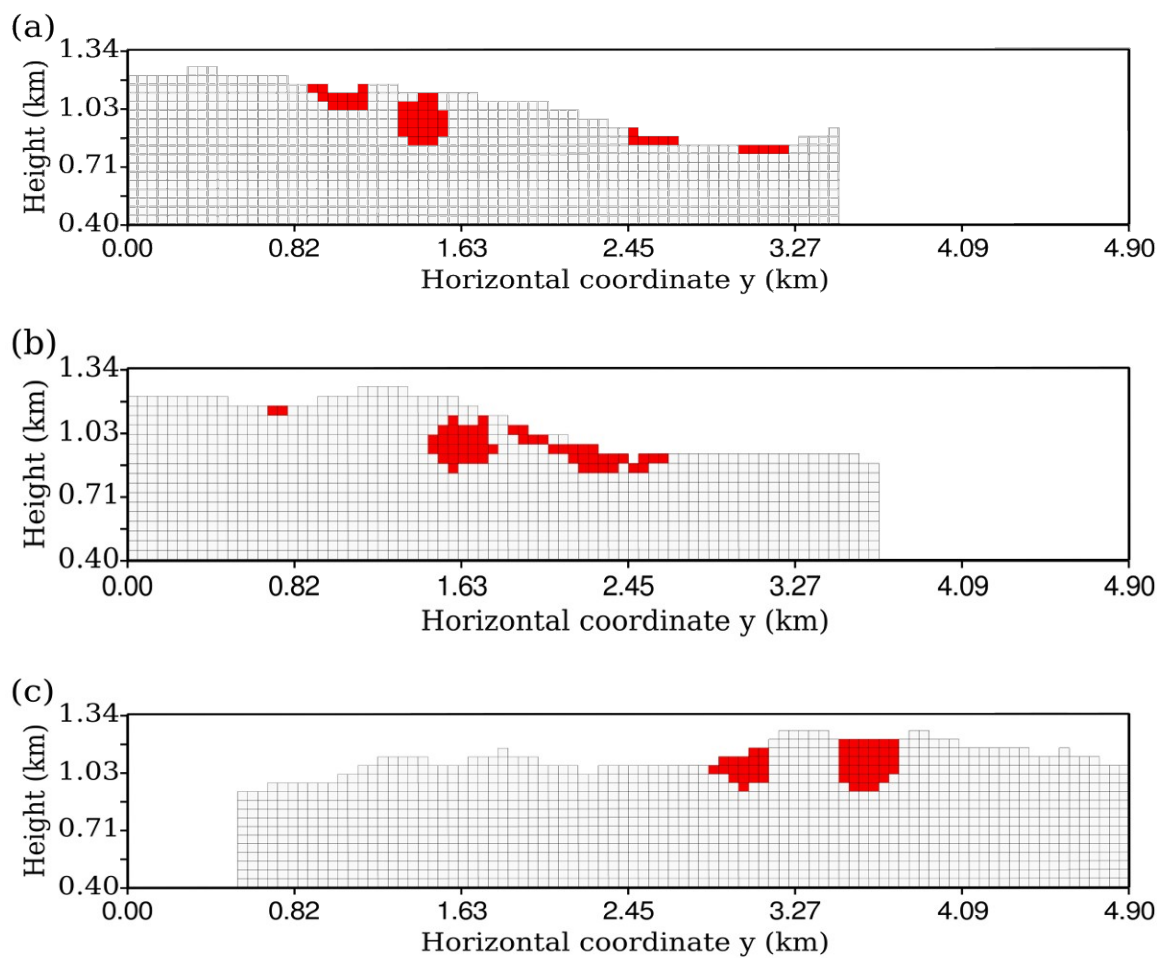


Figure 10. Results from the application to real data from the Quadrilátero Ferrífero, southeastern Brazil. The vertical axis refers to height above the ellipsoid. Cross-sections of the inversion result shown in Figure 9 at horizontal coordinate x equal to (a) 1.00 km, (b) 1.35 km, and (c) 5.55 km. Prisms with zero density contrast are shown in light gray and prisms with density contrast of 1.0 g/cm^3 , corresponding to the iron orebody, are shown in red.

CONCLUSIONS

We have presented a new method for the 3D inversion of gravity gradient data that uses a systematic search algorithm. We parametrized the Earth's subsurface as a grid of juxtaposed right rectangular prisms with homogeneous density contrasts. The estimated density-contrast distribution is then iteratively built through the successive accretion of new elements around user-specified prisms called "seeds". The choice of seeds is used to incorporate into the solution prior information about the density-contrast values and the approximate location of the sources. Our method is able to retrieve multiple sources with different locations, geometries, and density contrasts by allowing each seed to have a different density contrast. Furthermore, we devised a robust procedure that recovers only targeted sources in the presence of non-targeted sources that yield interfering gravitational effects. Thus, prior information about the non-targeted sources is not required and the gravitational effect of the targeted sources does not need to be previously isolated to perform the inversion. In real world scenarios, meeting both of the previously stated requirements would have been highly impractical, or even impossible.

The developed inversion method requires small processing time and low computer memory usage since there are neither matrix multiplications nor linear systems to be solved. Further computational efficiency is achieved by implementing a "lazy evaluation" of the Jacobian matrix. These optimizations make feasible the inversion of the large data sets brought forth by airborne gravity gradiometry surveys when using an interpretation model composed of a

large number of prisms. Tests on synthetic data and real data from an airborne gravity gradiometry survey show that our method is able to recover compact bodies with different density contrasts despite the presence of interfering gravitational effects produced by non-targeted sources.

Despite the advantages of this new inversion method, its use is restricted to areas where there is sufficient geologic information about the targeted sources. Estimating a correct density-contrast distribution requires adequate placement of the seeds and correct density-contrast values. Horizontal coordinates for the seeds can be easily obtained from the analysis of the g_{zz} component of the gravity gradient tensor. Approximate depths and density-contrast values for the seeds can be obtained from well data or previous interpretations of other geophysical data sets, like seismic or electromagnetic surveys. Therefore, given well constrained geologic information about the sources, our method is well suited for estimating the extent of structures of interest to mineral and hydrocarbon exploration, like salt domes and ore deposits.

ACKNOWLEDGEMENTS

We thank Vanderlei Coelho de Oliveira Junior and Dionisio Uendro Carlos for discussions and insightful comments. We acknowledge the use of plotting library matplotlib by Hunter (2007) and software Mayavi2 by Ramachandran and Varoquaux (2011). This research was supported by the Brazilian agencies CNPq and CAPES. The authors would like to thank Vale for permission to use the gravity gradiometry data of the Quadrilátero Ferrífero.

REFERENCES

- Camacho, A. G., F. G. Montesinos, and R. Vieira, 2000, Gravity inversion by means of growing bodies: *Geophysics*, **65**, 95–101, doi:10.1190/1.1444729.
- Claerbout, J.F., and F. Muir, 1973, Robust modeling with erratic data. *Geophysics*, **38**, 826-844, doi: 10.1190/1.1440378.
- Cox, L. H., G. Wilson, and M. S. Zhdanov, 2010, 3D inversion of airborne electromagnetic data using a moving footprint: *Exploration Geophysics*, **41**, 250–259, doi: 10.1071/EG10003.
- Guillen, A., and V. Menichetti, 1984, Gravity and magnetic inversion with minimization of a specific functional: *Geophysics*, **49**, 1354–1360, doi:10.1190/1.1441761.
- Hunter, J. D., 2007, Matplotlib: A 2D graphics environment: *Computing in Science and Engineering*, **9**, 90–95, doi:10.1109/MCSE.2007.55.
- Jorgensen, G. J., and J. L. Kisabeth, 2000, Joint 3D inversion of gravity, magnetic and tensor gravity fields for imaging salt formations in the deepwater Gulf of Mexico: 70th Annual International Meeting, SEG, Expanded Abstracts, 424–426.
- Krahenbuhl, R. A., and Y. Li, 2009, Hybrid optimization for lithologic inversion and time-lapse monitoring using a binary formulation: *Geophysics*, **74**, no. 6, I55–I65, doi:10.1190/1.3242271.
- Li, Y., 2001, 3D inversion of gravity gradiometer data: 71st Annual International Meeting, SEG, Expanded Abstracts, 1470–1473.

- Li, Y., and D. W. Oldenburg, 1998, 3-D inversion of gravity data: *Geophysics*, **63**, 109–119, doi: 10.1190/1.1444302.
- _____, 2003, Fast inversion of large-scale magnetic data using wavelet transforms and a logarithmic barrier method: *Geophysical Journal International*, **152**, 251–265, doi: 10.1046/j.1365-246X.2003.01766.x.
- Martinez, C., Y. Li, R. Krahenbuhl, and M. Braga, 2010, 3D Inversion of airborne gravity gradiometry for iron ore exploration in Brazil: 80th Annual International Meeting, SEG, Expanded Abstracts, 1753–1757.
- Menke, W., 1989, *Geophysical Data Analysis: Discrete Inverse Theory*, volume 45 of International Geophysics Series: Academic Press Inc.
- Nagihara, S., and S. A. Hall, 2001, Three-dimensional gravity inversion using simulated annealing: Constraints on the diapiric roots of allochthonous salt structures: *Geophysics*, **66**, 1438–1449, doi:10.1190/1.1487089.
- Nagy, D., G. Papp, and J. Benedek, 2000, The gravitational potential and its derivatives for the prism: *Journal of Geodesy*, **74**, 552–560, doi: 10.1007/s001900000116.
- Pedersen, L. B., and T. M. Rasmussen, 1990, The gradient tensor of potential field anomalies: Some implications on data collection and data processing of maps: *Geophysics*, **55**, 1558–1566, doi:10.1190/1.1442807.
- Pilkington, M., 1997, 3-D magnetic imaging using conjugate gradients: *Geophysics*, **62**, 1132–1142, doi: 10.1190/1.1444214.
- Portniaguine, O., and M. S. Zhdanov, 1999, Focusing geophysical inversion images: *Geophysics*, **64**, 874–887, doi: 10.1190/1.1444596.

- _____, 2002, 3-D magnetic inversion with data compression and image focusing: *Geophysics*, **67**, 1532–1541, doi: 10.1190/1.1512749.
- Ramachandran, P., and G. Varoquaux, 2011, Mayavi: 3D visualization of scientific data: *Computing in Science and Engineering*, **13**, 40–50, doi:10.1109/MCSE.2011.35
- René, R. M., 1986, Gravity inversion using open, reject, and “shape-of-anomaly” fill criteria: *Geophysics*, **51**, 988–994, doi:10.1190/1.1442157.
- Routh, P. S., G. J. Jorgensen, and J. L. Kisabeth, 2001, Base of the salt imaging using gravity and tensor gravity data: 71st Annual International Meeting, SEG, Expanded Abstracts, 1482–1484.
- Silva Dias, F. J. S., V. C. F. Barbosa, and J. B. C. Silva, 2007, 2D gravity inversion of a complex interface in the presence of interfering sources: *Geophysics*, **72**, no. 2, I13–I22, doi: 10.1190/1.2424545.
- _____, 2009, 3D gravity inversion through an adaptive-learning procedure: *Geophysics*, **74**, no. 3, I9–I21, doi:10.1190/1.3092775.
- _____, 2011, Adaptive learning 3D gravity inversion for salt-body imaging: *Geophysics*, **76**, no. 3, I49–I57, doi:10.1190/1.3555078.
- Silva, J. B. C., and V. C. F. Barbosa, 2006, Interactive gravity inversion: *Geophysics*, **71**, no 1, J1–J9, doi:10.1190/1.2168010.
- Silva, J. B. C., and A. O. Cutrim, 1989, A Robust Maximum Likelihood Method for Gravity and Magnetic Interpretation: *Geoexploration*, **26**, 1–31, doi: 10.1016/0016-7142(89)90017-3.

- Silva, J. B. C., and G. W. Holmann, 1983, Nonlinear magnetic inversion using a random search method: *Geophysics*, **48**, no. 12, 1645–1658.
- Tarantola, A., 2005, Inverse problem theory and methods for model parameter estimation: Society for Industrial and Applied Mathematics.
- Vasco, D. W., 1989, Resolution and variance operators of gravity and gravity gradiometry: *Geophysics*, **54**, 889–899, doi: 10.1190/1.1442717.
- Wilson, G.A., M. Cuma, and M.S. Zhdanov, 2011, Large-scale 3D Inversion of Airborne Potential Field Data: 73rd EAGE Conference & Exhibition incorporating SPE EUROPEC 2011, Expanded Abstracts, K047.
- Zhdanov, M. S., R.G. Ellis, and S. Mukherjee, 2004, Regularized focusing inversion of 3-D gravity tensor data: *Geophysics*, **69**, no. 04, 925–937, doi: 10.1190/1.1778236.
- Zhdanov, M. S., A. Green, A. Gribenko, and M. Cuma, 2010a, Large-scale three-dimensional inversion of Earthscope MT data using the integral equation method: *Physics of the Earth*, **8**, 27-35, doi: 10.1134/S1069351310080045.
- Zhdanov, M.S., X. Liu, and G. A. Wilson, 2010b, Rapid imaging of gravity gradiometry data using 2D potential field migration: 80th Annual International Meeting, SEG, Expanded Abstracts, 1132–1136.